Determining Spectral Response of the National Ignition Facility Particle Time of Flight Diagnostic to Xrays

B. Reichelt,[1, a)] N. Kabadi,[1] J. Pearcy,[1] M. Gatu Johnson,[1] S. Dannhoff,[1] B. Lahmann,[1] J. Frenje,[1] C. K. Li,[1] G. Sutcliffe,[1] J. Kunimune,[1] R. Petrasso,[1] H. Sio,[2] A. Moore,[2] E. Mariscal,[2] and E. Hartouni[2]
[1)] *Massachusetts Institute of Technology, Cambridge, Massachusetts 02139, USA*
[2)] *Lawrence Livermore National Laboratory, Livermore, California 94550, USA*

(Dated: 7 December 2023)

The Particle Time of Flight (PTOF) diagnostic is a chemical vapor deposition (CVD) diamond detector used for measuring multiple nuclear bang times at the National Ignition Facility (NIF). Due to the non-trivial, polycrystalline structure of these detectors, individual characterization and measurement is required to interrogate the sensitivity and behavior of charge carriers. In this paper, a process is developed for determining the xray sensitivity of PTOF detectors and relating it to intrinsic properties of the detector. We demonstrate that the diamond sample measured has a significant non-homogeneity in its properties, with the charge collection well described by a linear model $ax + b$, where $a = 0.63 \pm 0.16 V^{-1} mm^{-1}$ and $b = 0.00 \pm 0.04 V^{-1}$. We also use this method to confirm an electron to hole mobility ratio of 1.5 ± 1.0 and an effective band gap of $1.8eV$ rather than the theoretical $5.5eV$, leading to a large sensitivity increase.

I. INTRODUCTION

The Particle Time of Flight (PTOF) diagnostic is a diagnostic routinely utilized for measuring the time of peak nuclear emission for low yield implosions at the National Ignition Facility (NIF)[1]. PTOF relies upon a gold-coated chemical vapor deposition (CVD) grown diamond that has a bias held across it. Diamond is a good choice of detector in high energy density physics as its high bandgap of 5.5 eV and strong interatomic bonds lead to impressive radiation hardness and low leakage currents[2,3]. When ionizing radiation interacts with the biased diamond, an electron-hole pair is freed into the conduction/valence band, respectively. These freed charges are now mobile, and are swept in opposite directions by the bias, where they will induce a surface charge on the gold electrode and will either eventually recombine or get absorbed into the electrode. In either case, the resulting charges on the electrode will induce a change in voltage that can be read via an oscilloscope.

Despite being used for proton and neutron signals, PTOF is also sensitive to xrays. This fact is important in choosing the filtering, as an xray signal that is too large can lead to saturation and loss of the nuclear signal. Having an absolute calibration of the sensitivity to xrays will aide with filter selection and ensure data remains analyzable. Additionally, a better understanding of how PTOF reacts to xrays enhances the possibility of using PTOF for xray bang time information.

The xray response of PTOF also provides information about the behavior of charge carriers in CVD diamond, which is important for gaining a more accurate understanding of how the response of PTOF varies for different ionizing radiation. Most pertinently, neutrons deposit their energy volumetrically throughout the detector, whereas charged particles and xrays deposit more energy at the front of the detector since they are significantly attenuated by the diamond. The standard PTOF detector is biased at $0.5\ V/\mu m$ with a $1000\ \mu m$ thickness, significantly more than the charge collection distance[3], meaning that the region energy is deposited in can significantly alter sensitivity and the falling edge of the impulse response.

II. SOURCE CHARACTERIZATION

To test xray sensitivity, a Proto Xray cabinet (https://www.protoxrd.com) was used along with custom-machined hardware to mount the PTOF detector and an xray spectrometer. The xrays are generated by thick target bremsstrahlung of an electron beam with known energy and current. As the xrays exit the source window, they pass through a hole in a shielding plate 16 cm below the source, where they are filtered and collimated to obtain an appropriate photon flux for measurement (see fig 1). The collimators used are made with the tungsten based alloy HD17 and range in thickness from $1 - 2$ mm, while filtering was provided by well characterized aluminum disks of various thicknesses. Previous work using image plates has shown the source to be uniform within the collimated area. After passing through the filtering and collimation, the xrays deposit their energy in either a PTOF detector or calibrated spectrometer, which can easily be swapped out for each other. The collimation is chosen to ensure that the imaged source size on both devices is smaller than the active area of each device, ensuring accurate conversion between spectra measured by the spectrometer and those absorbed by the PTOF detector.

The PTOF detector tested utilizes a 10 mm diameter, 1 mm thick microwave plasma grown CVD diamond biased at 500 V. The "normal" bias direction is taken to

[a)] The author to whom correspondence may be addressed: blr@mit.edu

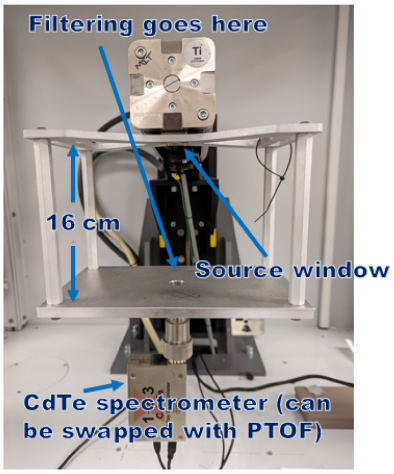

FIG. 1. Picture of the experimental setup, showing the xray source and hardware used to mount the spectrometer and PTOF detector in the same location.

be such that the front of the diamond facing the xray source is at a higher potential than the rear face. The diamond comes with a $9mm$ diameter metallization for biasing purposes on both sides, consisting of $100nm$ Ti for diamond adhesion, 200 nm Pt to inhibit diffusion from Ti into Au, and 1000 nm of Au to act as an electrode. Current through the PTOF detector at a given bias and xray spectrum was measured with a Keithley multi-meter. To probe response at different xray energies, a variety of sources, filtering, and electron beam voltages were utilized.

The spectra utilised in the analysis were measured with an Amptek X-123 CdTe spectrometer (https://www.amptek.com) mounted in nearly the same location as the PTOF detector. Energy axis calibration was achieved with a ^{241}Am source. Ideally, the spectrometer would be run with the exact same collimation and xray source current as the PTOF detector. Unfortunately, the precision of our electrometer was too low for this to be practical, since currents large enough to measure on the PTOF detector with the multimeter led to extreme pile-up on the spectrometer. Thus, the inital analysis step was to relate the magnitude of the spectrum to the collimation and xray source current used and to ensure that spectral shape was not significantly altered by changing these parameters.

Finding the scaling of the spectral magnitude with collimator size and xray source current involves a maximum likelihood fit between two spectra– the unscaled "reference spectrum" and the "scaled spectrum". Specifically, we take the high statistic reference spectrum and smooth slightly with a Gaussian filter before dividing by the live time in order to get a reference count rate for each bin. The desired scaling is applied by multiplying this reference rate by the scale factor A and fitting to the scaled spectrum until Poisson distributed log-likelihood is maximized. An example of scaled spectra is given in fig 2, where spectra taken with varying collimation and xray source current have been scaled to match a reference spectrum using the above process. Fig 2 demonstrates that aside from the $25\mu m$ collimation, spectral shape is conserved with different collimators.

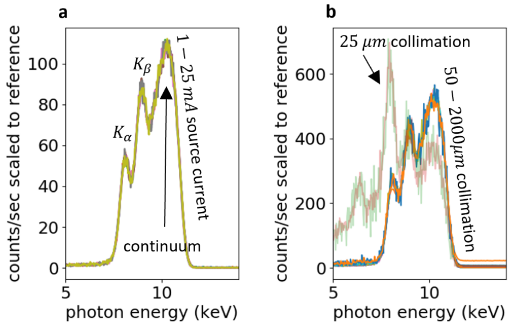

FIG. 2. Spectra scaled to match reference spectrum for Cu source with 140.1 mg/cm^2 Al filtering, varying a) source current from $1-25mA$ and b) collimation diameter from $25-2000\mu m$. Spectral shape is evidently independent of these parameters outside of $25\mu m$ collimation.

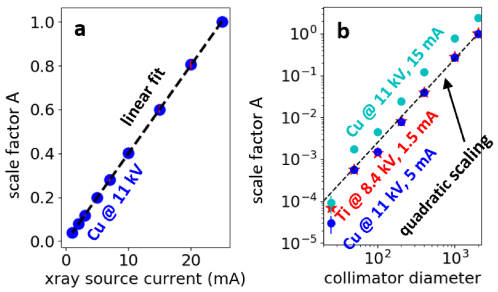

FIG. 3. Measured scalings of xray spectra vs a) xray source current, and b) collimator diameter. Note that the Cu points use Cu @ 11 kV, 5 mA with 2000 μm collimation as the reference, while the Ti points use Ti @ 8.4 kV, 1.5 mA with 2000 μm collimation as reference.

The results from scaling the source current and collimator diameter are shown in fig 3. It can be seen that the count rate for the Cu tube scales very linearly with the xray source current, with a Pearson correlation coefficient of 0.999989 (the Ti tube has a similar result). This simplifies conversion between spectrometer spectra and those incident upon the CVD diamond when they are taken at different source currents.

Meanwhile, the scaling for collimator size deviates much more noticeably from the quadratic scaling that would be expected from a point source. However, aside from the 25 μm collimator on the Cu tube, the shapes of all spectra match very well, and the deviations from quadratic scaling are well reproduced when changing source type, current, and voltage. The consistent nature of the shifts suggest some combination of finite source size

effects that are consistent between tubes and deviations in the collimator diameter from the nominal values.

The outliers are the 25 um collimators on the Cu tube, which had much lower count rates than expected and significantly distorted spectra. The most likely reason for this is that with an aspect ratio of 0.023, the smallest collimators were imaging an area with radius $\sim 3\ mm$– a size slightly smaller than the xray window size and less than half the radius imaged by all the other collimators. This made it extremely susceptible to misalignment, as only a 1° change could result in entirely missing the window. To aide with this, a smaller separation between the source and collimator stage will be used in future tests. To avoid this issue, on the current dataset only spectra taken with $\geq 50\ \mu m$ collimation are used.

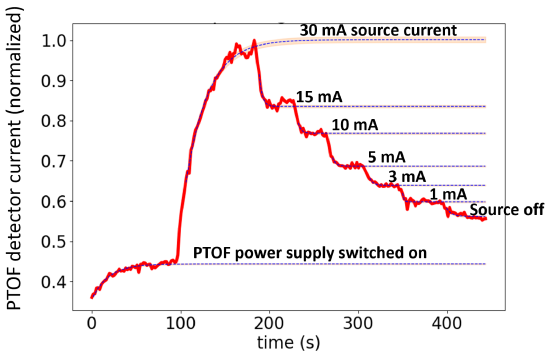

FIG. 4. Example trace of current through PTOF diamond. The xray source current is varied in steps and the PTOF current is given time to equilibrate at each step before being measured.

III. METHODOLOGY

The goal of these measurements is determine the sensitivity of the PTOF detector given some xray flux. To do this, we measure the current flowing through the detector over a series of steps in the xray source current, giving the detector $\sim 50s$ to equilibrate at each step. An example output trace is shown in fig 4. Ultimately, the current going through the detector, I_{PTOF}, is a function of the free carriers in the diamond:

$$I_{PTOF} = qA[v_e(n_e^{v,\gamma} + n_e^{t,\gamma} + n_e^{f,0}) + v_h(n_h^{c,\gamma} + n_h^{t,\gamma} + n_h^{f,0})] \quad (1)$$

with q being the electron charge, A being cross sectional area where carriers are present, and $v_{e(h)}$ the electron (hole) velocity, which is a function of electric field. The total free electron (hole) densities n_e and n_h are split into three components each: $n_{e(h)}^{v(c),\gamma}$ denotes the density of electrons (holes) excited by xrays from the valence (conduction) band to become free charge carriers, $n_{e(h)}^{t,\gamma}$ denotes the density of electrons (holes) excited by xrays from deeply trapped states to become free charge carriers, and $n_{e(h)}^{f,0}$ denotes the free carriers that are present when no xrays illuminate the diamond through thermal effects and shallow traps. All of the carrier parameters can be functions of location within the detector since they depend upon the local mobility and recombination rate of the diamond.

The $n_{e(h)}^{f,0}$ terms provide a continuous dark current and so aren't of primary interest for determining detector sensitivity to photons. Fig 4 displays an example PTOF current trace used for the analysis– the initial curve when the PTOF bias is applied demonstrates this dark current.

The $n_{e(h)}^{v(c),\gamma}$ terms are the ones we're most interested in since they provide the bulk of the charge carriers for high amplitude signals and scale linearly with xray flux[4]:

$$n_{e(h)}^{v(c),\gamma} = \frac{\tau_{e(h)} dP/dx}{A\epsilon} \quad (2)$$

Where x is distance from the front of the diamond, $dP/dx = \int_0^\infty P_0(E) e^{-\mu_C(E)x} \mu_C(E) dE$ is xray power absorbed per dx at position x given an initial spectrum P_0 at the front of the diamond and an xray attenuation factor[5] μ_C. Finally, ϵ is the number of eV required to free an electron-hole pair (previous analyses suggest 13 eV for diamond[6]).

The $n_{e(h)}^{t,\gamma}$ terms pose some difficulty since they obey a nonlinear rate equation[3]:

$$\frac{dn_{e(h)}^{t,\gamma}}{dt} = -(n_{e(h)}^{t,\gamma} + n_{e(h)}^{v(c),\gamma}) n_{e(h)}^{t,\gamma} \alpha^{RT} + (T - n_{e(h)}^{t,\gamma}) \frac{dP}{dx} \alpha^{DT} \quad (3)$$

Where α^{RT} and α^{DT} are the factors of the re-trapping and de-trapping frequencies not dependent on any carrier densities or xray flux, and T is the total density of trapped states. Guidance for analyzing this component can be found by considering the equilibrium solution:

$$n_{e(h)}^{t,\gamma} = \frac{1}{2}\sqrt{\left[\frac{dP}{dx}\left(\frac{\alpha^{DT}}{\alpha^{RT}} + \frac{\tau_{e(h)}}{A\epsilon}\right)\right]^2 + 4T\frac{dP}{dx}\frac{\alpha^{DT}}{\alpha^{RT}}} - \frac{1}{2}\frac{dP}{dx}\left(\frac{\alpha^{DT}}{\alpha^{RT}} + \frac{\tau_{e(h)}}{A\epsilon}\right) \quad (4)$$

We can see that for larger xray fluxes, this asymptotes to a value independent of xray flux, but at lower xray flux it quickly approaches zero. This is exactly the behavior seen in fig 4: when the source is turned off the current decays all the way down to the asymptotic dark current reached when turning on the power supply, albeit very slowly. Separate tests running for long periods of time have confirmed this experimentally. The slow decay at

the end agrees with eqn 3, which predicts a $1/t$ decay rather than an exponential once $dP/dx = 0$. Fully decoupling this term from the $n_{e(h)}^{v(c),\gamma}$ terms is difficult, but provided there is a large enough xray flux to saturate the trapped state component, it can be essentially absorbed into the intrinsic carrier population $n_{e(h)}^{f,0}$. Thus, we can write a linear relationship between current and power:

$$I_{PTOF} = \frac{q}{D}\int_0^D \frac{d(x)}{\epsilon(x)}\frac{dP}{dx}dx + I_{dark}\left(\int_0^t P(t')dt'\right) \quad (5)$$

Where the first term comes from spatially averaging eqn 1 over the diamond to get a spatially averaged charge collection $\langle qd/\epsilon D\rangle_x$ and the dark current is now a complex function of the total irradiation but remains nearly constant over each current trace when the source is on. D is the detector thickness and d is the charge collection distance and is nominally equal to $n_e^{v,\gamma}v_e + n_h^{c,\gamma}v_h$, but can deviate from this value near the contacts or in regions of strongly varying $v_{e(h)}$ or $n_{e(h)}^{v(c),\gamma}$.

In order to probe the detector response thoroughly, experimentation was done to find a combination of filterings and sources to create spectra with a variety of peaks. Smaller peaks are desirable to reduce analysis degeneracy but limitations on xray sources available to us necessitated filtering the continuum emission to get higher energy peaks. Fig 5 demonstrates the shape of the spectra used to determine sensitivity, as well as linear fits[7] relating source current to $I_{PTOF} - I_{dark}$ in the vein of eqn 5. Given the discussion of eqn 4, linear fits are taken only with the higher flux data points where possible to ensure saturation of trapped carriers. The discussion of trapped carriers is likely responsible for the notable difference in dark current between the Cu source and Ti sources, since that run was the first on the next day, after a large number of freed traps from heavy irradiation the prior day had time to recombine. Evidently, the xray flux for this shot alone was not high enough to re-saturate the freed traps over the course of the run.

IV. RESULTS

Using eqn 5, it is straightforward to postulate a linear charge collection model: $qd/\epsilon D = ax + b$. Combining with the formula for dP/dx, the spatially averaged charge collection becomes equivalent to a spectral average of the model sensitivity $S(E)$:

$$\left\langle \frac{qd}{\epsilon D}\right\rangle_x = \langle S\rangle_E = \int_0^\infty P_0 S(E)dE \Big/ \int_0^\infty P_0 dE \quad (6)$$

With $S(E) = (1 - e^{-\mu_C D})\left[a\mu_C^{-1} + b\right] - aDe^{-\mu_C D}$. However, we also know that the experimental sensitivity $(I_{PTOF} - I_{dark})/\int_0^\infty P_0 dE$ is a constant given by the lines fit in fig 5 b after some conversion to get from spectrometer measured spectra to those incident on PTOF

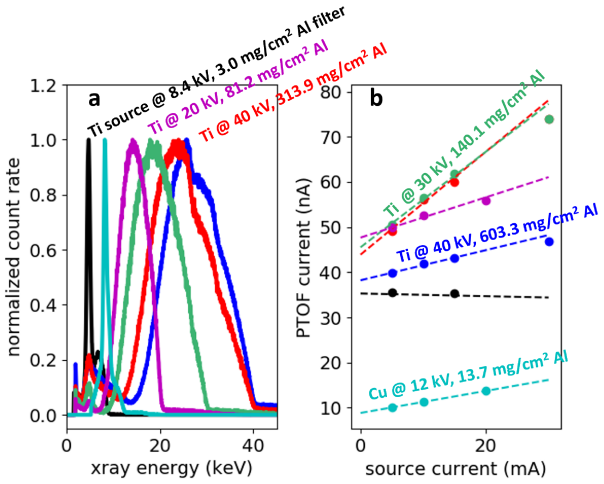

FIG. 5. Example illustrating a) normalized xray spectra and b) the corresponding PTOF currents. PTOF currents are plotted against a linear fit to the higher flux data points following the discussion of eqn 4. This fit is used to determine spectrally averaged sensitivity.

using methods from section II. The end result is that given a choice of a and b, we can see how well the averaged model sensitivities match the experimental values, and then perform a χ^2 minimization routine to select the optimal parameters.

The reasoning behind this linear charge collection model is that the diamond is not a perfect crystal– there are defects, impurities, and grain boundaries that alter the effective band gap and inhibit carrier movement[3]. The growth process for diamonds specifically results in an inhomogeneous structure as grain size grows from the nucleation side out. The best fit to a linear charge collection model leads to the blue model sensitivity curve and green averaged model sensitivities in fig 6. It can be seen that this does a good job at matching the experimental sensitivities, which are plotted against the averaged absorbed photon energy for the spectrum. Error bars from the experimental sensitivities come from the errors in the linear fits of source current vs detector current. This is added in quadrature with a 50% error attributed to the subtleties of eqn 4 that were sidestepped to get a linear fit– experimentation with fits to this equation assuming a simpler homogeneous model revealed departures of less than or similar to this from the linear fit. The exception is the Ti source @ 8.4 kV with $3.0 mg/cm^2$ Al filtering, whose error bar was chosen to match the signal level of the next smallest signal since it was at the noise floor and no discernible signal was present when the source was on.

The linear charge collection model $(q/D)(d/\epsilon) = ax+b$ has a best fit value of $a = 0.63 \pm 0.16 V^{-1}mm^{-1}$ and $b = 0.00 \pm 0.04 V^{-1}$, indicating spatial inhomogeneities are significant within this sample and suggesting the nucleation side of the diamond was the side facing the xray source. It is also clear that there are significant impurities and grain boundaries causing effective mod-

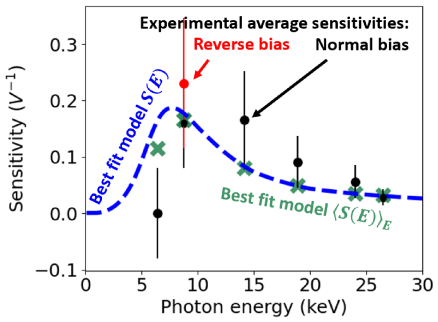

FIG. 6. Experimental sensitivities plotted vs mean absorbed photon energy for different spectra are plotted as the circular points. Shown in blue is the best fit model sensitivity curve $S(E)$, with the green x's being the spectrally averaged values. All measured spectra are corrected for attenuation through the contacts before being analyzed for sensitivity.

ification of the bandgap[8,9]– the standard value of q/ϵ in diamond is $0.077V^{-1}$, but this is exceeded by the end of the diamond where $(q/D)(d/\epsilon) \approx 0.6V^{-1}$. d/D must be less than unity, so the only way this can occur is if ϵ is smaller than usual owing to impurities. In fact, the difference is likely even more dramatic, as the usual values for carrier mobility and lifetimes in diamond[4,6] lead to $d/D \approx 0.1$. This is supported by the values of dark current observed: $I_{dark} \approx 10nA \approx 2qAv_e(m_e k_B T/2\pi\hbar^2)^{3/2} exp(-E_g/2k_B T)$ leads to a value of $E_g \approx 1.8eV$ rather than 5.5 eV.

Finally, one last notable feature of the data shown in fig 6 is the discrepancy between the forward and reverse bias configurations. In the forward bias configuration, the side nearest the source is biased higher than the rear side of the diamond. As just shown, there is greater carrier mobility at the rear side of the diamond so in the normal bias configuration the holes are moving in the direction of increasing mobility and lifetime, whereas the electrons are doing the opposite and so will recombine more quickly. The opposite is of course true for the reverse bias situation, and so the increased sensitivity is likely a result of greater electron mobility and lifetime. Taking an extreme model where $v_{e(h)}\tau_{e(h)} = 0$ in the forward (reverse) bias case so that $d \approx v_{h(e)}\tau_{h(e)}$, we obtain the charge collection ratio $v_e\tau_e/v_h\tau_h \approx 1.5\pm1.0$– in alignment with the ratio of electron to hole mobility discussed in the literature[4,6].

V. CONCLUSION AND PATH FORWARD

In conclusion, we have developed an in-house method for probing the behavior of PTOF detectors with xrays. Results with the current available detector show much higher sensitivity than expected, consistent with impurities introducing additional states for charge carriers within the band gap of the diamond. We also demonstrate the efficacy of a linear model in describing the charge collection of the diamond and provide a framework to disentangle the contributions of several different carrier species that contribute to xray response.

In the future, this process will be used to characterize both new and used PTOF detectors, and perform quality assurance. Additionally, experiments are currently underway to probe impulse response of these detectors using ultra short electron bunches at the LLNL xband facility. These tests will allow characterization of the carrier lifetimes, providing further insight into the mechanisms altering the sensitivity to low energy xrays. Future efforts will also be directed towards the intricacies of eqn 3 and lowering the error of this analysis through a combination of analytical models and improved equipment.

VI. DATA AVAILABILITY

The data that support the findings of this study are available from the corresponding author upon reasonable request.

ACKNOWLEDGMENTS

This work was supported by DOE/NNSA CoE contract DE-NA0003868 and LLNL contract B640112; B. Reichelt is supported by NNSA SSGF DE-NA0003960. Approved for unlimited release with release number LLNL-JRNL-835720.

[1] H. G. Rinderknecht *et al.*, "A novel particle time of flight diagnostic for measurements of shock- and compression-bang times in d3he and dt implosions at the nif," Review of Scientific Instruments **83**, 10D902 (2012), https://doi.org/10.1063/1.4731000.
[2] C. J. Wort and R. S. Balmer, "Diamond as an electronic material," Materials Today **11**, 22–28 (2008).
[3] D. Meier, *CVD Diamond Sensors for Particle Detection and Tracking*, Ph.D. thesis, Heidelberg U. (1999).
[4] D. R. Kania, L. S. Pan, P. Bell, O. L. Landen, H. Kornblum, P. Pianetta, and M. D. Perry, "Absolute x-ray power measurements with subnanosecond time resolution using type iia diamond photoconductors," Journal of Applied Physics **68**, 124–130 (1990), https://doi.org/10.1063/1.347104.
[5] R. T. Berger, "The x- or gamma-ray energy absorption or transfer coefficient: Tabulations and discussion," Radiation Research **15**, 1–29 (1961).
[6] C. Canali, E. Gatti, S. F. Kozlov, P. F. Manfredi, C. Manfredotti, F. Nava, and A. Quirini, "Electrical properties and performances of natural diamond nuclear radiation detectors," Nuclear Instruments and Methods **160**, 73–77 (1979).
[7] P. Virtanen *et al.*, "SciPy 1.0: Fundamental Algorithms for Scientific Computing in Python," Nature Methods **17**, 261–272 (2020).
[8] A. S. Moore, C. D. Bentley, J. M. Foster, G. Goedhart, P. Graham, M. J. Taylor, and E. Hellewell, "Soft x-ray measurements using photoconductive type-iia and single-crystal chemical vapor deposited diamond detectors," Review of Scientific Instruments **79**, 10E923 (2008), https://doi.org/10.1063/1.2966375.
[9] H. F. Haneef, A. M. Zeidell, and O. D. Jurchescu, "Charge carrier traps in organic semiconductors: A review on the underlying physics and impact on electronic devices," Journal of Materials Chemistry C **8**, 759–787 (2020).